universe

IMPACT FACTOR 2.9

CITESCORE 3.6

Article

Weak Coupling Regime in Dilatonic $f(R,T)$ Cosmology

Francisco A. Brito, Carlos H. A. B. Borges, José A. V. Campos and Francisco G. Costa

Special Issue
Universe: Feature Papers 2023—Cosmology

Edited by
Dr. Kazuharu Bamba

MDPI

https://doi.org/10.3390/universe10030134

universe

MDPI

Article

Weak Coupling Regime in Dilatonic $f(R,T)$ Cosmology

Francisco A. Brito [1,2,*], Carlos H. A. B. Borges [1,3], José A. V. Campos [2] and Francisco G. Costa [3]

[1] Departamento de Física, Universidade Federal da Paraíba, Caixa Postal 5008, João Pessoa 58051-970, Paraíba, Brazil; carlos.borges@ifpb.edu.br
[2] Departamento de Física, Universidade Federal de Campina Grande, Caixa Postal 10071, Campina Grande 58109-970, Paraíba, Brazil; a.campos@uaf.ufcg.edu.br
[3] Instituto Federal de Educação Ciência e Tecnologia da Paraíba (IFPB), Campus Campina Grande—Rua Tranquilino Coelho Lemos, 671, Jardim Dinamérica I, Campina Grande 58432-300, Paraíba, Brazil; francisco.geraldo@ifpb.edu.br
* Correspondence: fabrito@df.ufcg.edu.br

Abstract: We consider $f(R,T)$ modified theories of gravity in the context of string-theory-inspired dilaton gravity. We deal with a specific model that under certain conditions describes the late time Universe in accord with observational data in modern cosmology and addresses the H_0 tension. This is done by exploring the space of parameters made out of those coming from the modified gravity and dilatonic charge sectors. We employ numerical methods to obtain several important observable quantities.

Keywords: $f(R,T)$ gravity; dilatonic gravity; H_0 tension

Citation: Brito, F.A.; Borges, C.H.A.B.; Campos, J.A.V.; Costa, F.G. Weak Coupling Regime in Dilatonic $f(R,T)$ Cosmology. *Universe* **2024**, *10*, 134. https://doi.org/10.3390/universe10030134

Academic Editor: Kazuharu Bamba

Received: 18 December 2023
Revised: 4 March 2024
Accepted: 5 March 2024
Published: 11 March 2024

1. Introduction

Modern observations in cosmology, performed from Type Ia Supernova (SNIa) [1,2], Large Scale Structure (LSS) [3,4], Wilkinson Microwave Anisotropy Probe (WMAP) [5–7] data, Cosmic Microwave Background (CMB) [8,9] and Baryonic Acoustic Oscillations (BAO) [10,11], indicate that the expansion of the Universe has entered an accelerated phase. Furthermore, the same observational data show that 95% of the matter and energy content of the Universe (when described in terms of a fluid effectively entering Einstein's equations) is in the form of unknown species called Dark Matter (DM) and Dark Energy (DE). General Relativity has always been consistent with observational data and one of the most recent examples is the detection of gravitational waves through LIGO [12]. General Relativity analyzes the acceleration of the Universe based on dark energy, according to observations of type Ia supernovae, which counterbalances gravitational attraction. The Dark Energy [13–20] component (ρ_x) is characterized by a negative effective pressure, $p_x < -\rho_x/3$. The simplest candidate for such a dark energy is a positive cosmological constant Λ, but such an identification raises some difficult questions, such as why Λ is so small (in particle physics) [21–23]. This is called the fine-tuning problem for Λ. Another important problem is why $\Lambda = \rho_{x0}$ in present epoch (where ρ_{x0} is the present value of the dark energy density of the Universe, in Planck units). This problem is known as cosmic coincidence [24]. A promising way to solve the above problems is to introduce a single scalar field, dubbed the quintessence [25], whose potential goes asymptotically to zero. The potential associated with this scalar field tends to zero as the field goes to infinity after an infinite (very long) time. On the other hand, we can try to reconcile the observational data with the acceleration of the Universe through modifications of the theory of gravity. One way to do this is to start with a modification of the Einstein–Hilbert action formulation using an arbitrary function of the Ricci scalar, $f(R)$ [26]. In this context, we assume that at large scales the Einstein gravity model breaks down. Some specific types of $f(R)$ models have been proposed in the literature (see [27–29] and related references for a recent review). These theories acquired a lot of interest following the

work by Starobinsky on cosmic inflation [30]. The late-time cosmic acceleration of the Universe, in this context, was first explained by a natural modification, adding terms to the action that are proportional to R^n [31,32]. Quintessence issues by taking into account generic models with actions containing $f(R)$ terms were addressed in Ref. [33]. Quantum effects may lead to a generalization of $f(R)$ theories of gravity [34–36]. In Ref. [37], an unusual coupling between matter and geometry was developed by Harko et al., where the gravitational sector is given by an arbitrary function of the Ricci scalar and the trace T of the energy-momentum tensor. This type of theory is known as $f(R,T)$ gravity. Cosmological and astrophysical consequences of $f(R,T)$ models have been explored in the last few years. For instance, in Ref. [38], cosmological solutions for a perfect fluid in a spatially flat Friedmann–Lemàıtre–Robertson–Walker (FLRW) metric is investigated. Other studies on cosmological applications of $f(R,T)$ gravity, including the inflationary scenario, can be found in the Refs. [39–45]. An essential component of all superstring models, and consequently, of the cosmological scenarios based on the string effective action, is the dilaton field. This field controls the effective strength of all gauge couplings in the context of "grand-unified" models of all fundamental interactions [46]. This coupling strengths may drive the Universe towards a phase of strong coupling, which can possibly precede the standard decelerated evolution. The dilaton can also be geometrically interpreted as the effective "radius" of the eleventh dimension [47] in the M-theory context. The dilaton may control the inflationary dynamics and play a role in the generation of the primordial spectra of quantum fluctuations amplified by inflation. String theory dilaton may provide a natural implementation of the coupled quintessence scenario, provided the cosmological running of the dilaton does not stop after entering the weak coupling regime $e^{\phi} \ll 1$, as $\phi \to -\infty$. We shall consider a particular scenario in which the dilaton approaches to zero as $t \to \infty$. This is possible with an exponentially suppressed (non-perturbative) potential. As we shall see, because of the loop corrections, the fields inside the matter action are in general non-minimally and non-universally coupled to the dilaton. This will render dilatonic charge densities that are fundamental to form the new space of parameters of the model.

In Section 2, we will present the formalism of a theory of gravity modified by $f(R,T)$, addressing the variation of the modified action, while in Section 3, we will review a scenario of string theory at low energy $\phi \to -\infty$ with a dilatonic field subject to an effective potential $\tilde{V}$. In Section 4, we will analyze a dilatonic cosmological theory in a scenario of modified gravity of type $f(R,T)$ for a homogeneous and isotropic FLRW universe. Section 5 is dedicated to detail the evolution of cosmological relevant quantities through numerical methods. Our discussions and conclusions are, respectively, present in Sections 6 and 7.

2. Gravitational Field Equations of $f(R,T)$ Gravity

Let us first take the action given in [37]:

$$S = \frac{1}{2\kappa}\int d^4x f(R,T)\sqrt{-g} + \int d^4x \mathcal{L}_m \sqrt{-g}, \tag{1}$$

where $f(R,T)$ is an arbitrary function of the Ricci scalar curvature $R = g^{\mu\nu}R_{\mu\nu}$, $T = g^{\mu\nu}T_{\mu\nu}$ is the trace of the energy-momentum tensor and $\mathcal{L}_m$ is the Lagrangian density of matter and $\kappa = 8\pi G$.

Admitting the definition of the energy-momentum tensor, we can express it in such a way that the Lagrangian density of matter depends only on $g_{\mu\nu}$, that is:

$$T_{\mu\nu} = g_{\mu\nu}\mathcal{L}_m - 2\frac{\partial \mathcal{L}_m}{\partial g^{\mu\nu}}. \tag{2}$$

By varying the action given in Equation (1) in relation to $g^{\mu\nu}$, we have the field equations given by:

$$\begin{aligned} f_R(R,T)R_{\mu\nu} &+ g_{\mu\nu}\Box f_R(R,T) - \nabla_\mu\nabla_\nu f_R(R,T) \\ &+ f_T(R,T)(T_{\mu\nu}+\Theta_{\mu\nu}) - \frac{1}{2}f(R,T)g_{\mu\nu} - 8\pi T_{\mu\nu} = 0, \end{aligned} \tag{3}$$

so that $(T_{\mu\nu}+\Theta_{\mu\nu})$ corresponds to the variation of the trace with respect to the metric tensor, with $\Theta_{\mu\nu} \equiv g^{\alpha\beta}\,\dfrac{\delta T_{\alpha\beta}}{\delta g^{\mu\nu}}$ set in [37]. We will denote $f_R(R,T)$ and $f_T(R,T)$ as the derivatives of $f(R,T)$ with respect to the Ricci scalar curvature and the trace of the energy-momentum tensor, respectively.

From the definition of $\Theta_{\mu\nu}$ and using Equation (2), we have:

$$\Theta_{\mu\nu} = -2T_{\mu\nu} + g_{\mu\nu}\mathcal{L}_m - 2g^{\alpha\beta}\frac{\partial^2\mathcal{L}_m}{\partial g^{\mu\nu}\partial g^{\alpha\beta}}. \tag{4}$$

In other words, $\Theta_{\mu\nu}$ will depend on the Lagrangian of matter, which can refer to the case of the electromagnetic field, the massless scalar field and the case of the perfect fluid, among others.

3. Stringy Cosmology

Let us now consider cosmological scenarios related to the effective action that comes from low-energy string theory in which the dilaton field exerts influence in the dynamics of the Universe. We shall focus on the sector of the effective action, coming from a low-energy string theory, given by the tensor field (the metric $\tilde{g}_{\mu\nu}$) and a scalar field (the dilaton ϕ), where the tilde indicates that we are working on the *string frame*, and where the dilaton couples to the Ricci scalar and dilatonic dynamics in an explicit form—see below. Our starting point is the string-frame, low-energy, gravidilaton effective action, to the lowest order in the α' expansion, but including the dilaton-dependent loop and nonperturbative corrections, encoded in a few "form factors", due to the loop corrections $\psi(\phi)$ and $Z(\phi)$ [48]. $V(\phi)$ is the effective dilaton potential. The model action is [49,50]:

$$S = -\frac{M_P^2}{2}\int d^4x\sqrt{-\tilde{g}}\left[e^{-\psi(\phi)}\tilde{R} + \tilde{Z}(\phi)\left(\tilde{\nabla}\phi\right)^2 + \frac{2}{M_P^2}\tilde{V}(\phi)\right] + \tilde{S}_{\rm m}(\phi,\tilde{g},{\rm matter}). \tag{5}$$

We can discuss the phenomenology of the relic dilaton background by taking into account two possibilities. First, massive dilaton is gravitationally more *strongly coupled* to macroscopic matter. In strong coupling limit $\phi \to \infty$, we assume that it is possible to make an asymptotic Taylor expansion in inverse powers of the coupling constant $g_s^2 = \exp(\phi)$, similar to the context of "induced gravity". In these models, the gravitational and gauge couplings saturate at small, but finite, values because of the very large number N of fundamental gauge bosons presents in the loop corrections [49,50]. By this assumption, we can write $\exp(-\psi(\phi)) = c_1^2 + b_1\exp(-\phi)+\mathcal{O}(\exp(-2\phi))$, $Z(\phi) = -c_2^2 + b_2\exp(-\phi)+\mathcal{O}(\exp(-2\phi))$ and $\tilde{V} = V_0\exp(-\phi)+\mathcal{O}(\exp(-2\phi))$, where c_1^2 and c_2^2 are dimensionless numbers. To be consistent with the tree-level relation $\lambda_P/\lambda_S = M_S/M_P = \exp(\phi/2)$ (for $d=3$), in which $M_P \simeq 10M_S$, as required by a consistent string unification in the context of gravitational and gauge interactions [51], and we have $c_1^2 \sim c_2^2 \sim 10^2$. On the other hand, very light (or massless) dilaton is weakly coupled to matter. In the rest of this paper we will focus our attention on this second possibility, where we will consider that the dilaton is weakly coupled. In this regime, we will admit that $\phi \to -\infty$, while $\exp(-\psi(\phi)) = Z(\phi) = \exp(-\phi)$.

We can now characterize the dynamical evolution of the Universe with a metric minimally coupled to the dilaton. In this frame, the string effective action is also minimally coupled to perfect fluid sources. Considering the lowest order α', we have [49,50]:

$$S = -\frac{M_P^2}{2}\int d^4x\sqrt{-\tilde{g}}e^{-\phi}\left[\tilde{R} - \left(\tilde{\nabla}\phi\right)^2 + \frac{2}{M_P^2}\tilde{V}(\phi)\right] + \tilde{S}_m(\phi, \tilde{g}, \text{matter}). \tag{6}$$

We can use a more convenient coordinate system, the so-called *Einstein frame*, in terms of the metric $g_{\mu\nu}$ that is defined by a conformal transformation $\tilde{g}_{\mu\nu} = e^{\phi}g_{\mu\nu}$. In this frame, the action can be written as:

$$S = -\frac{M_P^2}{2}\int d^4x\sqrt{-g}\left[R - \frac{1}{2}(\nabla\phi)^2 + \frac{2}{M_P^2}\hat{V}(\phi)\right] + S_{\text{m}}(\phi, e^{\phi}g_{\mu\nu}, \text{matter}), \tag{7}$$

where we have defined:

$$\hat{V} = e^{\phi}\tilde{V}. \tag{8}$$

Because of the loop corrections, the fields appearing in the action S_{m} are generally non-minimally and non-universally coupled to the dilaton [52]. The gravitational and dilatonic "charge densities", $T_{\mu\nu}$ and σ, are defined as:

$$\frac{\delta S_{\text{m}}}{\delta g^{\mu\nu}} = \frac{1}{2}\sqrt{-g}T_{\mu\nu}, \quad \frac{\delta S_{\text{m}}}{\delta\phi} = \frac{1}{2}\sqrt{-g}\sigma. \tag{9}$$

When $\sigma \neq 0$, the effective gravidilaton theory is very different from a typical scalar-tensor gravity model of the Jordan–Brans–Dicke type.

4. Cosmology in Dilatonic $f(R, T)$ Gravity

Let us now assume that the action in Equation (6) depends not only on R, but on a function $f(R, T)$, so that R is the Ricci scalar curvature and T is the trace of the energy-momentum tensor of the dilatonic field. Since we are interested in investigating the dynamics of the dilaton field in the presence of other sources, we can rewrite this gravidilaton action as:

$$S = -\frac{M_p^2}{2}\int d^4x\sqrt{-g}f(R,T) + \frac{M_p^2}{2}\int d^4x\sqrt{-g}\left[\frac{1}{2}g^{\mu\nu}\nabla_\mu\phi\nabla_\nu\phi - \frac{2}{M_p^2}\hat{V}(\phi)\right] + S_{\text{m}}(\phi, e^{\phi}g_{\mu\nu}, \text{matter}). \tag{10}$$

Let us now assume a homogeneous and isotropic Universe described by the Friedmann–Lemàıtre–Robertson–Walker (FLRW) metric, whose line element is written as:

$$ds^2 = dt^2 - a^2(t)\left(dr^2 + r^2d\theta^2 + r^2\sin^2\theta\, d\phi^2\right). \tag{11}$$

In what follows, we will also consider $M_p^2 \equiv 1/8\pi G = 2$, except otherwise indicated. For this model, the dilatonic Lagrangian density $\mathcal{L}^{\phi}$ is given by:

$$\mathcal{L}^{\phi} = \frac{1}{2}g^{\mu\nu}\nabla_\mu\phi\nabla_\nu\phi - \hat{V}(\phi), \tag{12}$$

where $\hat{V}(\phi) = e^{\phi}\tilde{V}(\phi)$ is the effective dilaton potential as previously defined. The scalar dynamics of the model is governed by the energy-momentum tensor of the dilaton field and is given by:

$$T^{\phi}_{\mu\nu} = \nabla_\mu\phi\nabla_\nu\phi - g_{\mu\nu}\left[\frac{1}{2}g^{\alpha\beta}\nabla_\alpha\phi\nabla_\beta\phi - \hat{V}(\phi)\right], \tag{13}$$

from which we can write:

$$T^{\phi}_{00} = \frac{1}{2}\dot{\phi}^2 + \hat{V}(\phi), \tag{14}$$

$$T_{ii}^{\phi} = \frac{a^2}{2}\dot{\phi}^2 - a^2\hat{V}(\phi). \tag{15}$$

By tracing the energy-momentum tensor of the dilatonic field, we are left with:

$$T^{\phi} = -\dot{\phi}^2 + 4\hat{V}(\phi). \tag{16}$$

The dilaton equation of motion is given by:

$$\ddot{\phi} + 3H\dot{\phi} + \frac{d\hat{V}}{d\phi} + \frac{1}{2}\sigma = 0. \tag{17}$$

Following (9), σ is the charge associated with the coupling between dilatonic field and the fluid that makes up the Universe. In the usual way, $H = \dot{a}/a$ is the Hubble parameter and a dot denotes differentiation with respect to the Einstein cosmic time. For this model:

$$\rho_{\phi} = \frac{1}{2}\dot{\phi}^2 + \hat{V}(\phi), \qquad p_{\phi} = \frac{1}{2}\dot{\phi}^2 - \hat{V}(\phi), \tag{18}$$

are the energy density and pressure of the dilaton field.

Varying Equation (10) with respect to $g_{\mu\nu}$, we will obtain:

$$f_R(R,T)R_{\mu\nu} - \frac{1}{2}f(R,T)g_{\mu\nu} + (g_{\mu\nu}\Box - \nabla_\mu\nabla_\nu)f_R(R,T) = \frac{1}{2}T_{\mu\nu} - f_T(R,T)T_{\mu\nu} - f_T(R,T)\Theta_{\mu\nu}, \tag{19}$$

where $T_{\mu\nu} = T^f + T^{\phi}$ is total energy-momentum tensor of the perfect fluid (f) that fills the Universe (baryonic matter, radiation and dark matter) plus the dilaton field. Using Equation (4), we can write:

$$\Theta_{\mu\nu} = -2\left(T_{\mu\nu}^{\phi} + T_{\mu\nu}^{f}\right) + g_{\mu\nu}\left(\mathcal{L}^{\phi} + \mathcal{L}^{f}\right), \tag{20}$$

with $\mathcal{L}^{\phi}$ and $T_{\mu\nu}^{\phi}$ given by (12) and (18), respectively. We assume that the energy-momentum tensor of the matter and energy is given by $T_{\mu\nu} = (\rho + p)u_\mu u_{\mu\nu} - pg_{\mu\nu}$, with conditions $u_\mu u^\mu = 1$ and $u^\mu\nabla_\nu u_\mu = 0$ satisfied by the four-velocity u^μ. Therefore, the Lagrangian of the perfect fluid becomes $\mathcal{L}^f = -p$. In this way, we can write the $(0-0)$ and $(i-i)$ components of $\Theta_{\mu\nu}$ as:

$$\Theta_{00} = -\frac{1}{2}\dot{\phi}^2 - 3\hat{V} - 2\rho - p, \quad \Theta_{ii} = -\frac{3}{2}a^2\dot{\phi}^2 + 3a^2\hat{V} - a^2p. \tag{21}$$

In the following, we will consider a simple example of $f(R,T)$ theories in order to study the late time evolution of the Universe with the presence of a single dilatonic field.

4.1. Model $f(R,T) = R + \alpha T^{\phi}$

This model was first studied by Harko et al. in Ref. [37]. These authors reproduce, in the context of $f(R,T)$, a relativistically covariant model of interacting dark energy based on a specific action [53]. Another interesting aspect of this choice is that the gravitational coupling becomes an "effective time dependent coupling", depending on the derivative of $f(T)$ with respect to the trace [37]. In order to reconcile our model with the the evidences which support General Relativity, we will assume a modified gravity model by $f(R,T) = R + \alpha T$. Using the expression (19), we have:

$$R_{\mu\nu} - \frac{1}{2}g_{\mu\nu}R = \left(\frac{1}{2} - \alpha\right)T_{\mu\nu} - \alpha\Theta_{\mu\nu} + \frac{1}{2}g_{\mu\nu}\alpha T. \tag{22}$$

Thus, using the definitions (14)–(16) and (20) in (22), one can obtain $(0,0)$ and $(1,1)$ components of field equations in a FLRW Universe as being:

$$3H^2 = \left(\frac{1}{2} - \alpha\right)\frac{1}{2}\dot{\phi}^2 + \left(\frac{1}{2} + 4\alpha\right)\hat{V}(\phi) + \frac{1}{2}(1+3\alpha)\rho - \frac{1}{2}\alpha p, \tag{23}$$

$$2\dot{H} + 3H^2 = -\left(\frac{1}{2} + 3\alpha\right)\frac{1}{2}\dot{\phi}^2 + \left(\frac{1}{2} + 4\alpha\right)\hat{V}(\phi) - \frac{1}{2}(1+3\alpha)p + \frac{1}{2}\alpha\rho. \tag{24}$$

The combination of (23), (24) and (17) leads to the coupled conservation equations for the matter (baryonic and dark), radiation and dilaton energy density, respectively:

$$(1+3\alpha)\dot{\rho}_b + 3H(1+2\alpha)\rho_b + \alpha\left(12H\dot{\phi}^2 + 10\frac{d\hat{V}}{d\phi}\dot{\phi}\right) = 0, \tag{25}$$

$$(1+3\alpha)\dot{\rho}_d + \left[3(1+2\alpha)H - \frac{1}{2}(1-2\alpha)Q\dot{\phi}\right]\rho_d + \alpha\left(12H\dot{\phi}^2 + 10\frac{d\hat{V}}{d\phi}\dot{\phi}\right) = 0, \tag{26}$$

$$\left(1 + \frac{8}{3}\alpha\right)\dot{\rho}_r + 4(1+2\alpha)H\rho_r + \alpha\left(12H\dot{\phi}^2 + 10\frac{d\hat{V}}{d\phi}\dot{\phi}\right) = 0, \tag{27}$$

$$\dot{\rho}_\phi + 6H[\rho_\phi - (1+8\alpha)\hat{V}] - 10\alpha\frac{d\hat{V}}{d\phi}\dot{\phi} + \frac{1}{2}(1-2\alpha)\sigma\dot{\phi} = 0. \tag{28}$$

In the set of equations shown above, we have separate the radiation, baryonic and non-baryonic (dark) matter components of the cosmological fluid by setting:

$$\rho = \rho_m + \rho_r = \rho_b + \rho_d + \rho_r, \quad p_b = p_d = 0, \quad p_r = \frac{1}{3}\rho_r. \tag{29}$$

We assume that ordinary matter and radiation have nearly metric couplings, i.e., that σ_b and σ_r vanish as $\phi \to -\infty$. This agrees, for instance, with the precision tests of Newtonian gravity [54]. In the dark matter sector, we shall assume a specific model to Lagrangian density. For "cold dark matter", one has a dilatonic charge σ_d which gives us the relationship [49,50,55]:

$$Q(\phi) = \frac{\sigma_d}{\rho_d} = Q_0\frac{e^{Q_0\phi}}{c^2 + e^{Q_0\phi}}. \tag{30}$$

For large enough values of the constant c^2, $Q(\phi)$ approaches to finite (non-zero) values in the limit of weak coupling regime, that is, when $\phi \to -\infty$.

Finally, we shall specify the form of the effective (Einstein frame) dilaton potential by choosing the string frame potential as $\tilde{V}(\phi) = V_0$. This allows us to write, quite generically, the simplest potential:

$$\hat{V}(\phi) = V_0 e^{\phi}, \tag{31}$$

where V_0 is a constant. This potential is in agreement with the assumption of exponential suppression at weak coupling regime.

It is convenient to parameterize the temporal evolution of all variables in terms of the logarithm of the scale factor, $\chi = \ln(a/a_i)$. In this relationship, a_i corresponds to the initial scale factor. Thus, the Einstein Equation (23) and the dilaton Equation (17) can be written, respectively, as:

$$H^2 = \frac{(1+3\alpha)(\rho_b + \rho_d) + (1 + \frac{8}{3}\alpha)\rho_r + (1+8\alpha)\hat{V}}{6 - \left(\frac{1}{2} - \alpha\right)\left(\frac{d\phi}{d\chi}\right)^2}, \tag{32}$$

$$2H^2\frac{d^2\phi}{d\chi^2} + \left[(1+4\alpha)\left(\frac{1}{2}\rho_b + \frac{1}{2}\rho_d + \frac{1}{3}\rho_r\right) + (1+8\alpha)\hat{V} - 2\alpha H^2\left(\frac{d\phi}{d\chi}\right)^2\right]\frac{d\phi}{d\chi} + 2\frac{d\hat{V}}{d\phi} + Q\rho_d = 0. \tag{33}$$

The matter and radiation evolution equations become:

$$(1+3\alpha)\frac{d\rho_b}{d\chi}+3(1+2\alpha)\rho_b+\alpha\left[12H^2\left(\frac{d\phi}{d\chi}\right)^2+10\frac{d\hat{V}}{d\phi}\frac{d\phi}{d\chi}\right]=0, \tag{34}$$

$$(1+3\alpha)\frac{d\rho_d}{d\chi}+3(1+2\alpha)\rho_d-\frac{1}{2}(1-2\alpha)Q\rho_d\frac{d\phi}{d\chi}+\alpha\left[12H^2\left(\frac{d\phi}{d\chi}\right)^2+10\frac{d\hat{V}}{d\phi}\frac{d\phi}{d\chi}\right]=0, \tag{35}$$

$$\left(1+\frac{8}{3}\alpha\right)\frac{d\rho_r}{d\chi}+4(1+2\alpha)\rho_r+\alpha\left[12H^2\left(\frac{d\phi}{d\chi}\right)^2+10\frac{d\hat{V}}{d\phi}\frac{d\phi}{d\chi}\right]=0. \tag{36}$$

Finally, the dilaton conservation equation can be written as:

$$\frac{d\rho_\phi}{d\chi}+6[\rho_\phi-(1+8\alpha)\hat{V}]-10\alpha\frac{d\hat{V}}{d\phi}\frac{d\phi}{d\chi}+\frac{1}{2}(1-2\alpha)\sigma\frac{d\phi}{d\chi}=0, \tag{37}$$

which is equivalent to Equation (33). Finally, we defined the useful density parameter $\Omega=\rho/\rho_c$, where ρ_c is the critical energy density. Thus, Equation (32) can be rewritten in terms of different density parameters for each component of the Universe:

$$1=\Omega_r+\Omega_d+\Omega_b+\Omega_\phi, \tag{38}$$

where:

$$\Omega_r=\frac{\rho_r}{3H^2},\qquad \Omega_d=\frac{\rho_d}{3H^2},\qquad \Omega_b=\frac{\rho_b}{3H^2},\qquad \Omega_\phi=\frac{\rho_\phi}{3H^2}, \tag{39}$$

are the density parameters of radiation, dark matter, baryonic matter and dilaton field, respectively.

4.2. Numerics

We can solve the set of Equations (34)–(37) by numerical methods with Equation (32) as a constraint on the initial dataset. Here, we also recover the $8\pi G$ factor, which can be given in terms of the Planck mass $M_p\equiv 1/\sqrt{G}=1.22\times10^{19}$ GeV. We shall use a potential of the form (31), by assuming $V_0=2.65\times10^{-123}M_p^4$, as well as the $Q(\phi)$ Formula (30) with $c^2=10$ for different values of the charge Q_0.

As we shall see shortly, (α, Q_0) is the space of parameters that we will explore to address acceptable cosmological scenarios. To ensure that at the current time $\chi=0$, the values of the energy densities are in agreement with the data from current cosmological measurements, we adjust the initial values of the energy densities of radiation, dark matter, baryonic matter and dark energy, respectively, as $\rho_{ri}(\chi_i)=8.58\times10^{-93}M_p^4$, $\rho_{di}(\chi_i)=5.28\times10^{-98}M_p^4$, $\rho_{bi}(\chi_i)=9.30\times10^{-99}M_p^4$ and $\rho_{\phi i}(\chi_i)=1.67\times10^{-105}M_p^4$, starting the integration at $\chi_i=-20$—this corresponds to big bang nucleosynthesis (BBN) redshift $z_{\rm BBN}\sim10^9$. Furthermore, the initial value for the dilaton is $\phi_i=7\times10^{-8}M_p$.

5. Results

5.1. The Density Parameters Ω_r, Ω_d, Ω_b and Ω_ϕ

The density parameters (39) are depicted in Figures 1 and 2. The graph in Figure 1 expresses the behavior of the density parameter Ω of each component as a function of χ, by fixing $\alpha=2\times10^{-2}m_p^{-2}$ and adjusting scenarios with $Q_0=2$ and $Q_0=20$. Considering the radiation component Ω_r, we note that it presents a degenerate evolution that starts constantly between the intervals $\chi\approx[-20,-13]$, decays quickly between $\chi\approx[-15,-4]$ and becomes null outside both intervals. In other words, Q_0 does not interfere with the evolution of Ω_r. Regarding the dark matter component Ω_d, we have a degenerate behavior in the interval $\chi\approx[-20,-2]$ and a minimal influence of Q_0 on $\chi\approx[-2,1]$, in order to present a slightly more accentuated decay with the decrease of Q_0. In this curve, the evolution begins with $\Omega_d=0$ in the intervals $\chi\approx[-20,-13]$ and a sharp increase in $\chi\approx[-13,-2]$ that precede the decay; there is also a degenerate maximum point with $\Omega_d(\chi=-2)\approx0.9$. For the baryonic

matter component Ω_b, we have an evolution with a degeneracy in the interval $\chi \approx [-20, -1]$ and a sufficiently small influence of Q_0 outside this interval. The behavior of Ω_b starts with a null value at $\chi \approx [-20, -13]$ followed by a gentle increase, remaining constant at its maximum point with $\Omega_b = 0.15$ at $\chi \approx [-5, -2]$ and ends with a decay outside these ranges. Regarding the dilaton component Ω_ϕ, we have a beginning with $\Omega_\phi = 0$ that is independent of Q_0 in the interval $\chi \approx [-20, -2]$ and a significant elevation that grows smoothly with the increase in Q_0. Relating the components Ω_r, Ω_d and Ω_b, we note that at $\chi \approx -13$, the first decreases while the second and third increase. On the other hand, at $\chi \approx -2$, Ω_r remains null and Ω_d and Ω_b decrease while Ω_ϕ grows significantly, thus presenting an intersection with Ω_d at $\chi \approx -0.28$ and $\chi \approx -0.41$ for $Q_0 = 2$ and $Q_0 = 20$, respectively. We also have another point of intersection relating the components Ω_d and Ω_r given in $\chi \approx -8.01$ and $\chi \approx -7.97$ for $Q_0 = 2$ and $Q_0 = 20$, respectively.

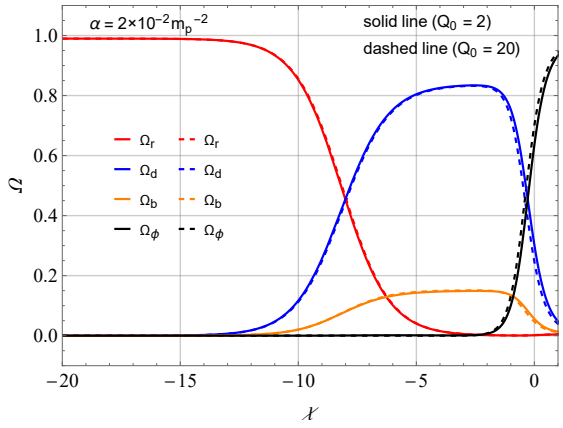

Figure 1. The density Ω as a function of χ for fixed $\alpha = 2 \times 10^{-2} m_p^{-2}$ and $Q_0 = 2$ and for $Q_0 = 20$.

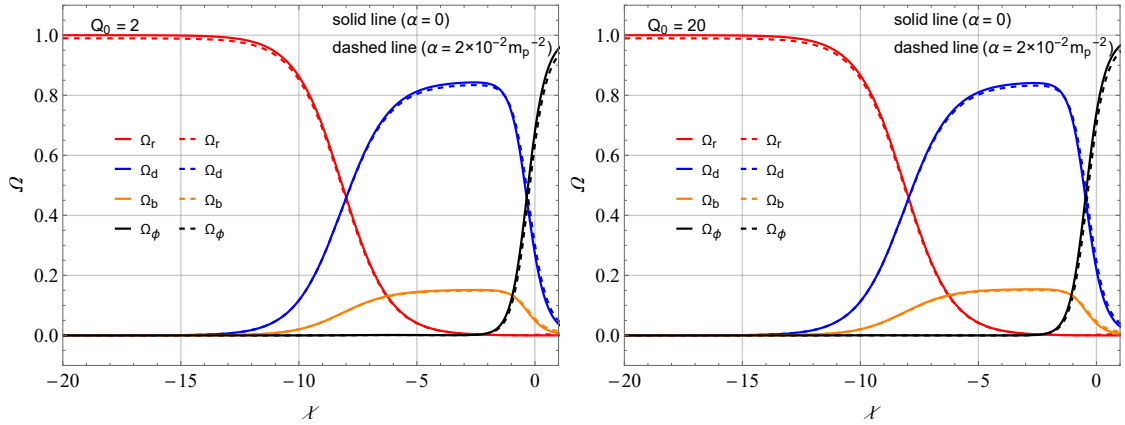

Figure 2. (**left panel**) The density Ω as a function of χ for fixed $Q_0 = 2$ and (**right panel**) $Q_0 = 20$ for $\alpha = 0$ and $\alpha = 2 \times 10^{-2} m_p^{-2}$.

The graphs in Figure 2 (left panel) and Figure 2 (right panel) are similar to each other; however, in Figure 2 (right panel), we set $Q_0 = 20$ and adjust α for two values as in Figure 2 (left panel). Comparing these graphs with Figure 1, we can observe that the increase in Q_0 has minimal influence on the radiation Ω_r, dark matter Ω_d and baryonic Ω_b components. However, for the dilaton component Ω_ϕ, we note that there is a more pronounced rise in the respective evolution curve.

5.2. The Hubble Parameter $H(z)$

The graph in Figure 3 expresses the behavior of the Hubble parameter as a function of redshift z, where we fixed $Q_0 = 2$ and explored different values for α. In this case, we can observe that in all values admitted for α we have a decay followed by an increase. Note that the minimum point of each curve has a redshift z that decreases with the increase in α, that is, for $\alpha = 0$, $\alpha = 5 \times 10^{-3} m_p^{-2}$, $\alpha = 1 \times 10^{-2} m_p^{-2}$ and $\alpha = 2 \times 10^{-2} m_p^{-2}$, we have $z \approx 0.64$, $z \approx 0.61$, $z \approx 0.59$ and $z \approx 0.54$, respectively. On the other hand, the values of the Hubble parameter at $z = 0$, i.e., H_0 increases with the growth of α, assuming values between $H_0 \approx 67$ km s^{-1} Mpc^{-1} and $H_0 \approx 72$ km s^{-1} Mpc^{-1}.

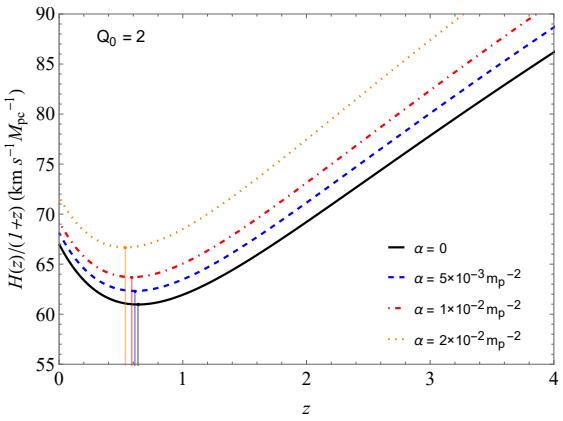

Figure 3. The Hubble parameter $H(z)$ as a function of the redshift z for fixed $Q_0 = 2$ and several values of α.

The graphs in Figure 4 show opposite behavior of the graph shown in Figure 3 with respect to the parameters, where they have interchanged their roles. More specifically, Figure 4 (left panel) shows the behavior of the Hubble parameter as a function of redshift z for different values of Q_0, for $\alpha = 0$ fixed. Notice that in all curves, we have a decay of H followed by an increase in which there is a degeneracy starting at $z \approx 2.6$. For $Q_0 = 2$, $Q_0 = 6$, $Q_0 = 10$ and $Q_0 = 20$, we have a minimum point at $z \approx 0.64$, $z \approx 0.69$, $z \approx 0.76$ and $z \approx 0.85$, respectively. We also note that the values of z, referring to each point of minimum, increase with the increase of Q_0. It is also worth noting that the decay of H to the minimum point becomes more pronounced with the increase of Q_0; additionally, for smaller values of Q_0, we have slower decays. In this case, the values of the Hubble parameter at $z = 0$, i.e., H_0 assume values between $H_0 \approx 67$ km s^{-1} Mpc^{-1} and $H_0 \approx 74$ km s^{-1} Mpc^{-1}. Finally, with respect to the graph in Figure 4 (right panel), we find that it is similar to Figure 4 (left panel), but with $\alpha = 5 \times 10^{-3} m_p^{-2}$ fixed. In this case, we again have a decay followed by an increase that becomes degenerate at $z \approx 2.4$. The curves assume minimum points whose redshift values are $z \approx 0.61$, $z \approx 0.67$, $z \approx 0.74$ and $z \approx 0.82$ corresponding to $Q_0 = 2$, $Q_0 = 6$, $Q_0 = 10$ and $Q_0 = 20$, respectively. We can see that H increases with the increase in α, and consequently, its minimum points take on greater values for H; however, the corresponding redshift values z decrease. Thus, in this case, the values of the Hubble parameter at $z = 0$, i.e., H_0 assume values between $H_0 \approx 68$ km s^{-1} Mpc^{-1} and $H_0 \approx 75.5$ km s^{-1} Mpc^{-1}.

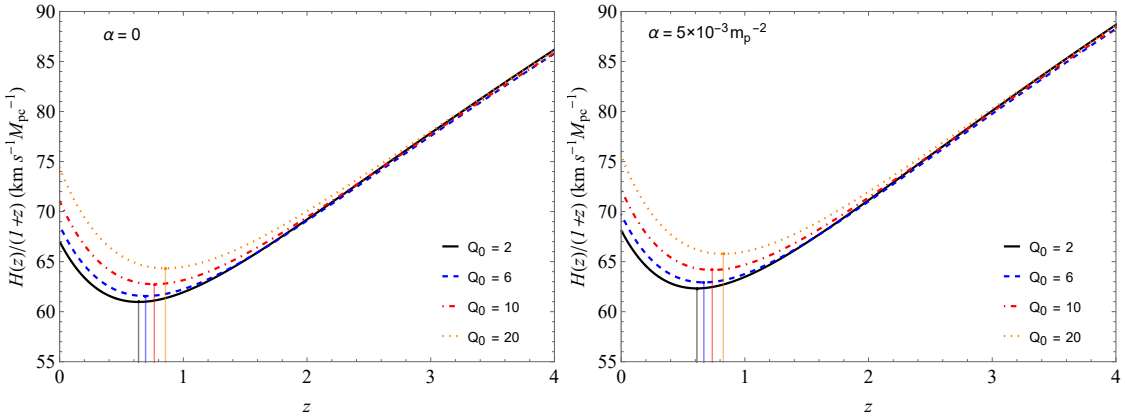

Figure 4. (**left panel**) The Hubble parameter $H(z)$ as a function of the redshift z for fixed $\alpha = 0$ and (**right panel**) $\alpha = 5 \times 10^{-3} m_p^{-2}$ and several values of Q_0.

5.3. The Dilaton Field

The graph in Figure 5 details the behavior of ϕ as a function of χ assuming $\alpha = 2 \times 10^{-2} m_p^{-2}$ being fixed and exploring different values for Q_0. In this case, there is a convergence of $\phi(\chi) = 0$ for each Q_0 in the interval $\chi \approx [-20, -13]$, followed by a decay that ends in $\phi(\chi \approx 1) = -10$. Notice that, in the range $\chi \approx [-10, -1]$, $\phi(\chi)$ presents a decay that becomes more pronounced with the decrease of Q_0, that is, the growth of Q_0 reflects a slower decay to $\phi(\chi)$. This can be observed more clearly by analyzing the decay in which $Q_0 = 20$, where $\phi(\chi \approx -7.5) \approx -1.5$ and $\phi(\chi \approx -2) \approx -2$, while for $Q_0 = 6$, we have $\phi(\chi \approx -8) \approx -1.5$ and $\phi(\chi \approx -7.3) \approx -2$. We also observe that from $\chi \approx -1$, we have an expressive decay that is independent of Q_0.

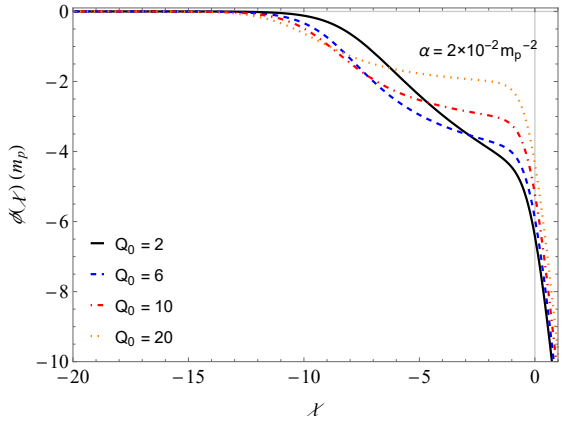

Figure 5. The dilaton field ϕ as a function of χ for fixed $\alpha = 2 \times 10^{-2} m_p^{-2}$ and several values of Q_0.

The graphs in Figure 6 are quite similar. In the first case (left panel), we fix $Q_0 = 2$ and explore three values for α. As we can see, the variation of α presents a sufficiently small change in the behavior of $\phi(\chi)$ that decays in a degenerate way in the interval $\chi \approx [-20, -1]$, while for the range $\chi \approx [-1, 1]$, we have a decay that becomes smoothly slower with increasing α. In the second case (right panel), we fix $Q_0 = 20$ and explore three values for α. Furthermore, we note that the increase in Q_0 contributes to a slower decay in the interval $\chi \approx [-20, -1]$.

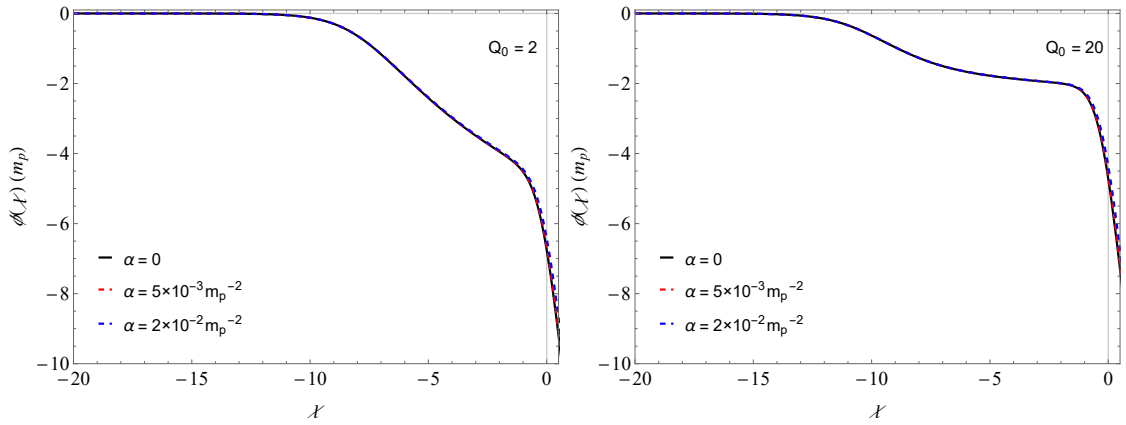

Figure 6. (**left panel**) The dilaton field ϕ as a function of χ for fixed $Q_0 = 2$ and (**right panel**) $Q_0 = 20$ and several values of α.

5.4. The Running of $Q(\phi)$

The graphic in Figure 7 represents the behavior of $Q(\phi)$ as a function of χ by considering different values for Q_0 and fixing $\alpha = 2 \times 10^{-2} m_p^{-2}$. Notice that for $Q_0 = 2$, we have a very slow decay in the interval $\chi \approx [-20, 0]$; however, it is more pronounced outside this range. Concerning the other curves, we have a decay that becomes more accentuated with the increase of Q_0 admitting $\chi \approx [-20, -1]$. Outside this range, we have an even more significant decay.

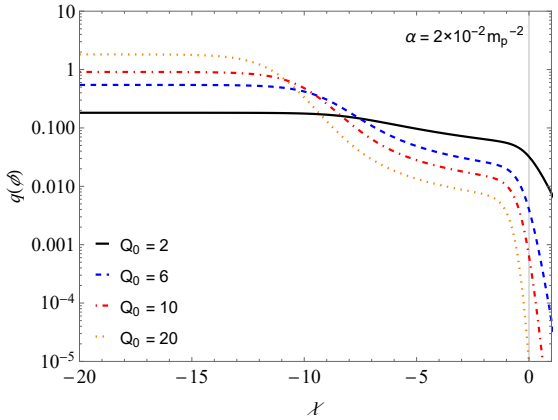

Figure 7. The evolution of $Q(\phi)$ as a function of χ for fixed $\alpha = 2 \times 10^{-2} m_p^{-2}$ and several values of Q_0.

The graphs in Figure 8 develops similar behavior. In the first case (left panel), we keep $Q_0 = 2$ fixed and explore some values of α. We note that $Q(\phi)$ decays degenerately in the interval $\chi \approx [-20, -1]$, that is, without any influence of α. Outside this range, $Q(\phi)$ decays more slowly with increasing α. In the second case (right panel), we keep $Q_0 = 20$ fixed and also explore some values of α and we have a degenerate decay that becomes slower with the increase of Q_0 and without the influence of α, in the range $\chi \approx [-20, -1]$; however, outside this range, we have a sharp decay that increases smoothly with the decrease in α.

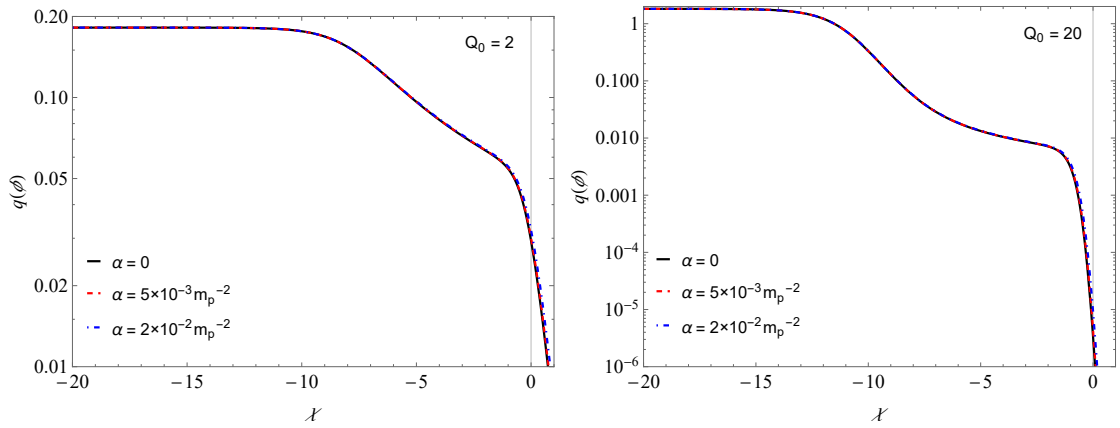

Figure 8. (**left panel**) The evolution of $Q(\phi)$ as a function of χ for fixed $Q_0 = 2$ and (**right panel**) $Q_0 = 20$ and several values of α.

5.5. The Energy Densities ρ_r, ρ_d, ρ_b and ρ_ϕ

The graphs in Figure 9 show the evolution of energy density as a function of χ for each component. In the first case (left panel), we fix $Q_0 = 2$ and consider $\alpha = 0$ and $\alpha = 2 \times 10^{-2} m_p^{-2}$. Notice that for $\alpha = 0$, the components of radiation ρ_r and dark matter ρ_d and baryonic ρ_b present a linear decay, so that for ρ_r, we have a more pronounced behavior in relation to ρ_d and ρ_b. On the other hand, assuming $\alpha = 2 \times 10^{-2} m_p^{-2}$, we will have degenerate models at $\alpha = 0$ in the intervals $\chi \approx [-16, -1]$, $\chi \approx [-20, 1]$ and $\chi \approx [-20, 0.5]$, for ρ_r, ρ_d and ρ_b, respectively. Outside these ranges, each component decays more slowly, so that ρ_r, ρ_d and ρ_b converge their energies after $\chi \approx 3$. For the dilaton component, ρ_ϕ, we have a degenerate decay and non-linear scenarios, considering both α. Such decay becomes slower after $\chi \approx -3$, thus presenting points of intersection with each of the other components, that is, at $\chi \approx -2.5$, $\chi \approx -1$ and $\chi \approx -0.5$ we have the points of intersection between the decays of ρ_ϕ with ρ_r, ρ_b and ρ_d, respectively. Similar behavior can be found for the second case (right panel) for $Q_0 = 20$.

Furthermore, in relation to the dilaton component ρ_ϕ (right panel), it presents a more pronounced decay when compared to the graph in (left panel), that is, ρ_ϕ has a more significant decay with the increase Q_0. For the points of intersection between ρ_ϕ and the other components, we will have the same values corresponding to χ; however, such points occur at a lower energy density when compared to the graph in (left panel).

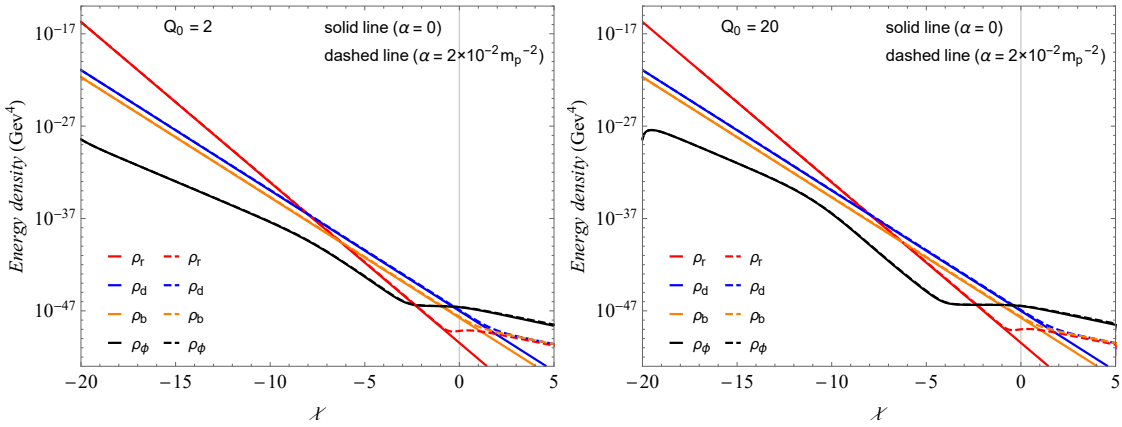

Figure 9. (**left panel**) The evolution of the energy densities for different components as a function of χ for fixed $Q_0 = 2$ and (**right panel**) $Q_0 = 20$ for two values of α.

6. Discussions

We shall first address the issue of H_0 tension. This problem now well known as the "Hubble tension" is related to the divergence of the measurements of the Hubble constant H_0 with respect to different applied techniques. In other words, the measurements of regions in the recent Universe, such as observations from the Hubble Space Telescope of Cepheid variables—see Riess et al. [56,57]—present considerable different results for H_0 as compared with its measurements made in the early Universe by the Planck spacecraft—for the 2018 Planck release, see [58]. The main difference between these two techniques is that in the latter case, the data from Planck CMB observations are processed under the base-ΛCDM model. This has raised some questions about this model and then some extended models have been put forward in the literature in order to solve the "Hubble tension", but according to the analysis performed in [58], none of the extended models solves this tension in a satisfactory way. In our present study, we also offer an alternative model to address this problem. We have considered three region of parameters to accomplish both techniques. We denominate these sets of parameters as scenarios I, II and III—see Table 1 and Figures 3 and 4.

Table 1. Comparison of the ranges of H_0 values obtained by Riess et al. 2019 [56] and Planck 2018 [58] with Scenarios I, II and III obtained by numerical methods through the parameters $\alpha = 0$, $\alpha = 2 \times 10^{-2} m_p^{-2}$, $\alpha = 5 \times 10^{-2} m_p^{-2}$, $Q_0 = 2$ and $Q_0 = 20$. The entire range of values of H_0 in Riess et al. 2019 is included in the range of values set out in Scenario III and partially included in the range of values in Scenario II. As for the range of H_0 values for Planck, these partially comprise Scenarios I, II and III.

Experiments	H_0	α	Q_0
Riess et al. 2019 [56]	74.03 ± 1.42 km s^{-1} Mpc^{-1}	–	–
Planck 2018 [58]	67.3 ± 1.20 km s^{-1} Mpc^{-1}	–	–
Scenarios	H_0	α	Q_0
I	$67 - 72$ km s^{-1} Mpc^{-1}	$0 - 2 \times 10^{-2} m_p^{-2}$	2
II	$67 - 74$ km s^{-1} Mpc^{-1}	0	2–20
III	$68 - 76$ km s^{-1} Mpc^{-1}	$5 \times 10^{-3} m_p^{-2}$	2–20

Scenarios I and II, following the range of parameters properly chosen, can simulate the results from Riess et al. [56,57] and Planck-based ΛCDM model. Scenario III simulates Riess et al. [56,57]. Although this seems to be a reasonable test of viability of our model, a statistical analysis to find the best fit of α and Q_0 according to Planck data should be addressed elsewhere. A similar behavior in easing the Hubble constant tension has recently appeared in the context of W_3 algebras [59].

Concerning the densities Ω_r, Ω_d, Ω_b and Ω_ϕ, depicted in Figures 1 and 2 and Table 2, notice that for the regimes of parameters considered in the Scenario I, II and III, there are no significant changes in relation to the Planck-based ΛCDM model, although they yield substantial changes for the Hubble constant H_0.

Table 2. The table shows the values of density parameters for radiation, dark matter, baryonic matter and dilaton field (dark energy) at $\chi = 0$ for different regions in the space of parameters (α, Q_0).

Ω_r	Ω_d	Ω_b	Ω_ϕ	α	Q_0
9.4×10^{-5}	0.271	0.049	0.679	0	2
7.7×10^{-5}	0.219	0.040	0.740	0	20
16.2×10^{-5}	0.302	0.056	0.636	$2 \times 10^{-2} m_p^{-2}$	2
19.7×10^{-5}	0.266	0.047	0.701	$2 \times 10^{-2} m_p^{-2}$	20

The dilaton field is running to achieve the limit $\phi \to -\infty$ in all scenarios discussed above, as depicted in Figures 5 and 6, which guarantees the weak field field regime as we have previously assumed. Thus, the dilatonic potential (31) approaches zero at this limit, as expected in quintessence scenarios.

The initial values of the energy densities adopted above leads to acceptable current energy densities. For instance, for fixed parameters $\alpha = 0, Q_0 = 2$, at $\chi = 0$, we find $\rho_r = 3.44 \times 10^{-51}\text{GeV}^4$, $\rho_d = 9.87 \times 10^{-48}\text{GeV}^4$, $\rho_b = 1.79 \times 10^{-48}\text{GeV}^4$ and $\rho_\phi = 2.47 \times 10^{-47}\text{GeV}^4$. The matter–radiation equality occurs in the redshift z_{eq}. See in Table 3 different values for such redshift, the Hubble constant H_0 and a_{eq} for some region of parameters.

Table 3. The table shows the acceptable values of redshift of matter–radiation equality $z_{eq} \sim 3000$ and corresponding a_{eq}, and the Hubble constant H_0 for different regions in the space of parameters (α, Q_0). For $\alpha \neq 0$, one finds unacceptable values $z_{eq} \ll 3000$. This may be a sign that a statistical analysis can reveal that the best fit for α is very small or identically zero.

z_{eq}	H_0	a_{eq}	α	Q_0
3391	67.0	2.9×10^{-4}	0	2
3346.6	74.4	3.0×10^{-4}	0	20
604.1	68.1	16.5×10^{-4}	5×10^{-3}	2
425.6	75.5	23.4×10^{-4}	5×10^{-3}	20

7. Conclusions

We explore a model of string-theory-inspired dilaton gravity in realm of modified $f(R, T)$ gravity. The numerical analyses were made in the model and revealed several cosmological quantities to describe dark energy for the late-time Universe. The model displays linear contributions in T (trace of the energy-momentum tensor) and in this preliminary approach, it seems to cover the well-accepted behavior of ΛCDM model for low redshifts, which is in accord with the Planck 2018 data. In this perspective, the model also mimics extensions of the ΛCDM model due to suitable adjusted space of parameters that allows to deal with the Hubble constant H_0 tension. We have shown in three scenarios considered in the present study that by varying appropriately some parameters, such as α and Q_0, one can obtain values of H_0 in a wide range spanning from the Planck results to the SHOES results and beyond. The analysis on the redshift of matter–radiation equality shows better results for $\alpha = 0$. This may be a sign that a statistical analysis can reveal that the best fit for α is very small or identically zero. Although this seems to be a reasonable test of viability of our model, a statistical analysis to find the best fit of α and Q_0 according to Planck data should be addressed elsewhere. As a perspective, we shall address these and other issues in the future. Further studies with different models should be addressed, as for instance, one could apply several investigations on the inflationary regime, such as constraining the parameters through contour plot in the plane made out of scalar spectral indices and tensor-to-scalar ratio [60].

Author Contributions: F.A.B., C.H.A.B.B. and F.G.C. developed the conceptual idea; J.A.V.C. developed the numerics. All authors have read and agreed to the published version of the manuscript.

Funding: This research was funded by CNPq grant number 309092/2022-1, CNPq/PRONEX/FAPESQ-PB grant number 165/2018 and FAPESQ-PB grant number 77/2022. C.H.A.B. Borges also acknowledges PIQIFPB for financial support, PIQIFPB grant number 23325.003350.2022-84

Data Availability Statement: Data are contained within the article.

Conflicts of Interest: The authors declare no conflicts of interest.

References

1. Riess, A.G.; Filippenko, A.V.; Challis, P.; Clocchiatti, A.; Diercks, A.; Garnavich, P.M.; Gilliland, R.L.; Hogan, C.J.; Jha, S.; Kirshner, R.P.; et al. Observational evidence from supernovae for an accelerating universe and a cosmological constant. *Astron. J.* **1998**, *116*, 1009. [CrossRef]
2. Perlmutter, S.; Aldering1, G.; Goldhaber, G.; Knop, R.A.; Nugent, P.; Castro, P.G.; Deustua1, S.; Fabbro, S.; Goobar, A.; Groom, D.E.; et al. Measurements of Ω and λ from 42 High-Redshift Supernovae. *Astrophys. J.* **1999**, *517*, 565. [CrossRef]
3. Koivisto, T.; Mota, D.F. Dark energy anisotropic stress and large scale structure formation. *Phys. Rev. D* **2006**, *73*, 083502. [CrossRef]
4. Daniel, S.F.; Caldwell, R.R.; Cooray, A.; Melchiorri, A. Large scale structure as a probe of gravitational slip. *Phys. Rev. D* **2008**, *77*, 103513. [CrossRef]
5. Komatsu, E.; Kogut, A.; Nolta, M.R.; Bennett, C.L.; Halpern, M.; Hinshaw, G.; Jarosik, N.; Limon, M.; Meyer, S.S.; Page, L.; et al. First-year Wilkinson microwave anisotropy probe (wmap)* observations: Tests of Gaussianity. *Astrophys. J. Suppl.* **2003**, *148*, 119–134. [CrossRef]
6. Spergel, D.N.; et al. [WMAP Collaboration]. First-Year Wilkinson Microwave Anisotropy Probe (WMAP)* Observations: Determination of Cosmological Parameters. *Astrophys. J. Suppl.* **2003**, *148*, 175. [CrossRef]
7. Hinshaw, G.; Larson, D.; Komatsu, E.; Spergel, D.N.; Bennett, C.; Dunkley, J.; Nolta, M.R.; Halpern, M.; Hill, R.S.; Odegard, N.; et al. Nine-year Wilkinson Microwave Anisotropy Probe (WMAP) observations: Cosmological parameter results. *Astrophys. J. Suppl.* **2013**, *208*, 19. [CrossRef]
8. Caldwell, R.R.; Doran, M. Cosmic microwave background and supernova constraints on quintessence: Concordance regions and target models. *Phys. Rev. D* **2004**, *69*, 103517. [CrossRef]
9. Huang, Z.Y.; Wang, B.; Abdalla, E.; Su, R.K. Holographic explanation of wide-angle power correlation suppression in the cosmic microwave background radiation. *J. Cosmol. Astropart. Phys.* **2006**, *0605*, 013. [CrossRef]
10. Eisenstein, D.J.; Zehavi, I.; Hogg, D.W.; Scoccimarro, R.; Blanton, M.R.; Nichol, R.C.; Scranton, R.; Seo, H.J.; Tegmark, M.; Zheng, Z.; et al. Detection of the baryon acoustic peak in the large-scale correlation function of SDSS luminous red galaxies. *Astrophys. J.* **2005**, *633*, 560. [CrossRef]
11. Percival, W.J.; Reid, B.A.; Eisenstein, D.J.; Bahcall, N.A.; Budavari, T.; Frieman, J.A.; Fukugita, M.; Gunn, J.E.; Ivezić, Ž.; Knapp, G.R.; et al. Baryon acoustic oscillations in the Sloan Digital Sky Survey data release 7 galaxy sample. *Mon. Not. R. Astron. Soc.* **2010**, *401*, 2148. [CrossRef]
12. Abbott, B.P.; et al. [LIGO Scientific Collaboration and Virgo Collaboration]. Observation of Gravitational Waves from a Binary Black Hole Merger. *Phys. Rev. Lett.* **2016**, *116*, 061102. [CrossRef]
13. Padmanabhan, T. Dark energy and gravity. *Gen. Relativ. Gravit.* **2008**, *40*, 529–564. [CrossRef]
14. Frieman, J.; Turner, M.; Huterer, D. Dark Energy and the Accelerating Universe. *Ann. Rev. Astron. Astrophys.* **2008**, *46*, 385–432. [CrossRef]
15. Martin, J. Quintessence: A mini-review. *Mod. Phys. Lett. A* **2008**, *23*, 1252–1265. [CrossRef]
16. Caldwell, R.R.; Kamionkowski, M. The Physics of Cosmic Acceleration. *Ann. Rev. Nucl. Part. Sci.* **2009**, *59*, 397–429. [CrossRef]
17. Silvestri, A.; Trodden, M. Approaches to Understanding Cosmic Acceleration. *Rep. Prog. Phys.* **2009**, *72*, 096901. [CrossRef]
18. Bamba, K.; Capozziello, S.; Nojiri, S.; Odintsov, S.D. Dark energy cosmology: The equivalent description via different theoretical models and cosmography tests. *Astrophys. Space Sci.* **2012**, *342*, 155–228. [CrossRef]
19. Li, M.; Li, X.-D.; Wang, S.; Wang, Y. Dark Energy: A Brief Review. *Front. Phys.* **2013**, *8*, 828–846. [CrossRef]
20. Sami, M.; Myrzakulov, R. Late time cosmic acceleration: ABCD of dark energy and modified theories of gravity. *Int. J. Mod. Phys. D* **2016**, *25*, 1630031. [CrossRef]
21. Peebles, P.J.E.; Ratra, B. The Cosmological Constant and Dark Energy. *Rev. Mod. Phys.* **2003**, *75*, 559–606. [CrossRef]
22. Padmanabhan, T. Cosmological constant: The Weight of the vacuum. *Phys. Rep.* **2003**, *380*, 235–320. [CrossRef]
23. Sahni, V. The Cosmological constant problem and quintessence. *Class. Quant. Grav.* **2002**, *19*, 3435–3448. [CrossRef]
24. Velten, H.E.; Vom Marttens, R.F.; Zimdahl, W. Aspects of the cosmological "coincidence problem". *Eur. Phys. J. C* **2014**, *74*, 3160. [CrossRef]
25. Tsujikawa, S. Quintessence: A Review. *Class. Quant. Grav.* **2013**, *30*, 214003. [CrossRef]
26. Buchdahl, H.A. Non-linear Lagrangians and cosmological theory. *Mon. Not. R. Astron. Soc.* **1970**, *150*, 1–8. [CrossRef]
27. Sotiriou, T.P.; Faraoni, V. $f(r)$ theories of gravity. *Rev. Mod. Phys.* **2010**, *82*, 451. [CrossRef]
28. Nojiri, S.; Odintsov, S.D. Unified cosmic history in modified gravity: From F(R) theory to Lorentz non-invariant models. *Phys. Rept.* **2011**, *505*, 59–144. [CrossRef]
29. Nojiri, S.; Odintsov, S.D.; Oikonomou, V.K. Modified Gravity Theories on a Nutshell: Inflation, Bounce and Late-time Evolution. *Phys. Rept.* **2017**, *692*, 1–104. [CrossRef]
30. Starobinsky, A.A. A new type of isotropic cosmological models without singularity. *Phys. Lett. B* **1980**, *91*, 99–102. [CrossRef]
31. Carroll, S.M.; Duvvuri, V.; Trodden, M.; Turner, M.S. Is cosmic speed-up due to new gravitational physics? *Phys. Rev. D* **2004**, *70*, 043528. [CrossRef]
32. Nojiri, S.; Odintsov, S.D. Modified gravity with negative and positive powers of the curvature: Unification of the inflation and of the cosmic acceleration. *Phys. Rev. D* **2003**, *68*, 123512. [CrossRef]

33. Capozziello, S.; Cardone, V.F.; Carloni, S.; Troisi, A. Curvature quintessence matched with observational data. *Int. J. Mod. Phys. D* **2003**, *12*, 1969–1982. [CrossRef]
34. Dzhunushaliev, V.; Folomeev, V.; Kleihaus, B.; Kunz, J. Modified gravity from the quantum part of the metric. *Eur. Phys. J. C* **2014**, *74*, 2743. [CrossRef]
35. Yang, R. Effects of quantum fluctuations of metric on the universe. *Phys. Dark Universe* **2016**, *13*, 87. [CrossRef]
36. Liu, X.; Harko, T.; Liang, S.D. Cosmological implications of modified gravity induced by quantum metric fluctuations. *Eur. Phys. J. C* **2016**, *76*, 420. [CrossRef]
37. Harko, T.; Lobo, F.S.; Nojiri, S.I.; Odintsov, S.D. $f(R,T)$ gravity. *Phys. Rev. D* **2011**, *84*, 024020. [CrossRef]
38. Shabani, H.; Farhoudi, M. $f(R,T)$ cosmological models in phase space. *Phys. Rev. D* **2013**, *88*, 044048. [CrossRef]
39. Xu, M.X.; Harko, T.; Liang, S.D. Quantum Cosmology of $f(R,T)$ gravity. *Eur. Phys. J. C* **2016**, *76*, 449. [CrossRef]
40. Moraes, P.H.R.S.; Sahoo, P.K. The simplest non-minimal matter-geometry coupling in the $f(R,T)$ cosmology. *Eur. Phys. J. C* **2017**, *77*, 480. [CrossRef]
41. Shabani, H.; Ziaie, A.H. Bouncing cosmological solutions from $f(R,T)$ gravity. *Eur. Phys. J. C* **2018**, *78*, 397. [CrossRef]
42. Debnath, P.S. Bulk viscous cosmological model in $f(R,T)$ theory of gravity. *Int. J.Geom. Meth. Mod. Phys.* **2019**, *16*, 1950005. [CrossRef]
43. Bhattacharjee, S.; Sahoo, P. Comprehensive analysis of a non-singular bounce in $f(R,T)$ gravitation. *Phys. Dark Universe* **2020**, *28*, 100537. [CrossRef]
44. Bhattacharjee, S.; Santos, J.R.L.; Moraes, P.H.R.S.; Sahoo, P.K. Inflation in $f(R,T)$ gravity. *Eur. Phys. J. Plus* **2020**, *135*, 576. [CrossRef]
45. Gamonal, M. Slow-roll inflation in $f(R,T)$ gravity and a modified Starobinsky-like inflationary model. *Phys. Dark Universe* **2021**, *31*, 100768. [CrossRef]
46. Witten, E. Some properties of O (32) superstrings. *Phys. Lett. B* **1984**, *149*, 351–356. [CrossRef]
47. Witten, E. String theory dynamics in various dimensions. *Nucl. Phys. B* **1995**, *443*, 85–126. [CrossRef]
48. Damour, T.; Polyakov, A.M. The String dilaton and a least coupling principle. *Nucl. Phys. B* **1994**, *423*, 532. [CrossRef]
49. Gasperini, M. Dilatonic interpretation of quintessence? *Phys. Rev. D* **2001**, *64*, 043510. [CrossRef]
50. Gasperini, M.; Piazza, F.; Veneziano, G. Quintessence as a runaway dilaton. *Phys. Rev. D* **2001**, *65*, 023508. [CrossRef]
51. Veneziano, G. Large N bounds on, and compositeness limit of, gauge and gravitational interactions. *J. High Energy Phys.* **2002**, *6*, 051. [CrossRef]
52. Taylor, T.R.; Veneziano, G. Dilaton couplings at large distances. *Phys. Lett. B* **1988**, *213*, 459. [CrossRef]
53. Poplawski, N.J. A Lagrangian description of interacting dark energy. *arXiv* **2006**, arXiv:gr-qc/0608031.
54. Fischbach, E.; Talmadge, C. Six years of the fifth force. *Nature* **1992**, *356*, 207–215. [CrossRef]
55. Gasperini, M. On the response of gravitational antennas to dilatonic waves. *Phys. Lett. B* **1999**, *470*, 67–72. [CrossRef]
56. Riess, A.G.; Casertano, S.; Yuan, W.; Macri, L.M.; Scolnic, D. Large Magellanic Cloud Cepheid Standards Provide a 1% Foundation for the Determination of the Hubble Constant and Stronger Evidence for Physics beyond ΛCDM. *Astrophys. J.* **2019**, *876*, 85. [CrossRef]
57. Riess, A.G.; Yuan, W.; Macri, L.M.; Scolnic, D.; Brout, D.; Casertano, S.; Jones, D.O.; Murakami, Y.; Anand, G.S.; Breuval, L.; et al. A Comprehensive Measurement of the Local Value of the Hubble Constant with 1 km s^{-1} Mpc^{-1} Uncertainty from the Hubble Space Telescope and the SH0ES Team. *Astrophys. J. Lett.* **2022**, *934*, L7. [CrossRef]
58. Aghanim, N.; et al. [Planck]. Planck 2018 results. VI. Cosmological parameters. *Astron. Astrophys.* **2020**, *641*, A6; Erratum in *Astron. Astrophys.* **2021**, *652*, C4. [CrossRef]
59. Ambjorn, J.; Watabiki, Y. Easing the Hubble constant tension. *Mod. Phys. Lett. A* **2022**, *37*, 2250041. [CrossRef]
60. Santos, J.R.L.; da Costa, S.S.; Santos, R.S. Cosmological models for f(R,T)−Λ(ϕ) gravity. *Phys. Dark Univ.* **2023**, *42*, 101356. [CrossRef]